This is a peer-reviewed, accepted author manuscript of the following article: Carruthers, H., Clark, D., Clarke, F., Faulds, K., & Graham, D. (2020). Comparison of Raman and near-infrared chemical mapping for the analysis of pharmaceutical tablets. *Applied Spectroscopy*. https://doi.org/10.1177/0003702820952440

Comparison of Raman and Near-Infrared Chemical Mapping for the Analysis of Pharmaceutical Tablets

Hannah Carruthers[1,2], Don Clark[2], Fiona Clarke[2], Karen Faulds[1], Duncan Graham[1]

[1]University of Strathclyde, Department of Pure and Applied Chemistry, George Street, Glasgow, G1 1RD, UK.

[2]Pfizer Ltd., Ramsgate Road, Sandwich, CT19 9NJ, UK.

Abstract

Raman and near-infrared chemical mapping are widely used methods in the pharmaceutical industry to understand the distribution of components within a drug product. Recent advancements in instrumentation have enabled the rapid acquisition of high-resolution images. The comparison of these techniques for the analysis of pharmaceutical tablets have not recently been explored and thus the relative performance of each technique is not currently well defined. Here the differences in the chemical images obtained by each method are assessed and compared with scanning electron microscopy with energy dispersive X-ray microanalysis (SEM-EDX), as an alternative surface imaging technique to understand the ability of each technique to acquire a chemical image representative of the sample surface. It was found that the Raman data showed the best agreement with the spatial distribution of components observed in the SEM-EDX images. Quantitative and qualitative comparison of the Raman and near-infrared images revealed a very different spatial distribution of components with regards to domain size and shape. The Raman image exhibited sharper and better discriminated domains of each component whereas the near-infrared image was heavily dominated by large pixelated domains. This study demonstrated the superiority of using Raman chemical mapping compared with near-infrared chemical mapping to produce a chemical image representative of the sample

surface using routinely available instrumentation to obtain a better approximation of domain size and shape. This is fundamental for understanding knowledge gaps in current manufacturing processes; particularly relating the relationship between components in the formulation, processing condition and final characteristics. By providing a means to more accurately visualise the components within a tablet matrix, these areas can all be further understood.

Keywords: Raman mapping, Near-infrared mapping, NIR mapping, chemical imaging, pharmaceuticals, Scanning electron microscopy, energy dispersive X-ray microanalysis, pharmaceutical tablets, imaging tablets.

Introduction

Raman and near-infrared (NIR) chemical mapping are closely related tools for characterising the spatial distribution of components within pharmaceutical tablets. Recent advancements of spectroscopic mapping equipment have enabled enhanced spatial resolution to be achieved in a reduced time improving the information that can be extracted from chemical images.[1] The relative capabilities of each technique have not been recently compared for the analysis of pharmaceutical products, thus the performance of each method is not currently well understood. To overcome the limitations in knowledge, this study assesses the ability of each technique to obtain a chemical image representative of a sample surface.

Šašić previously compared the two chemical mapping methods in 2007 for the analysis of common pharmaceutical tablets.[2] This study reported that all components could be successfully identified using Raman chemical mapping, however NIR mapping could only locate half of the components. This was expected due to the enhanced resolution obtainable using Raman spectroscopy. However, comparison of the chemical images revealed little difference in the distribution of components

obtained by each technique with regards to the domain size and shape. It is thought that the combination of the higher spatial resolution available using a Raman confocal microscope, with the recent advancements of rapid Raman data collection, will enable better discrimination between individual components and reveal information on the size and shape of domains. Šašić, however, did not determine if the chemical images obtained accurately represented the sample composition and distribution. In the presented study, we compare the chemical images acquired with alternative surface imaging techniques (scanning electron microscopy with energy dispersive X-ray microanalysis, SEM-EDX) to determine which vibrational spectroscopic method produces component images most accurately representing the real sample surface.

SEM-EDX analysis is an alternative surface imaging tool that can be used to examine the spatial distribution of components within a tablet matrix.[3] Backscattered electron (BSE) compositional imaging mode allows variations in atomic number to be easily visualised *via* a contrast map of the specimen, where bright areas correspond to regions of high atomic number and vice versa.[4] BSE images cannot in themselves identify what elements are present, however it can locate dissimilar elements within a sample. EDX microanalysis can be used as a complementary technique to determine the elemental composition of those regions which may then be used to identify components of a known formulation.[5] However, this method can only be used for samples whose components differ in their elemental composition and thus usually struggles to differentiate between organic excipients. Spectroscopic mapping is therefore the favoured method of visualising the microstructure of a tablet matrix. Recent publications have demonstrated the value in coupling Raman mapping and SEM-EDX analysis as complementary tools to characterise the distribution of components within a tablet matrix.[6] This has drawn a lot of interest in recent years

and led to the development of SEM-Raman mapping systems which combines confocal Raman mapping and scanning electron microscopy within a single microscope system.[7]

Both Raman and NIR chemical images are currently used in the pharmaceutical industry to visualise formulation composition. To date, applications have included formulation development,[8, 9] process understanding[10 - 14] and characterising out of specification batches.[15, 16] An overview of the literature suggests NIR chemical mapping has been more extensively explored within the pharmaceutical industry.[17]

Raman and NIR spectroscopy are complementary techniques where functional groups that exhibit an intense Raman signal, generally give a weak NIR response and vice versa.[18, 19] The sensitivity of each technique for a particular formulation will therefore depend on the chemical nature of the individual components.

Pharmaceutical formulations generally consist of a combination of an active pharmaceutical ingredient (API) and inactive substances that provide the formulation with its desired physical and manufacturing properties. Generally, APIs are organic compounds that usually contain aromatic and / or olefin functionality and are microcrystalline in nature. Raman spectroscopy is typically better for identifying low concentration APIs with small particle sizes due to the shaper bands present in Raman spectra, and the smaller collection volume it offers.[20]

Pharmaceutical excipients generally vary in nature ranging from organic to inorganic, crystalline to amorphous as well as different hydration states. Many frequently used excipients are derived from carbohydrates, such as celluloses, sugars and starches. Although these compounds exhibit very different functions within a tablet formulation, their chemical structures are often very similar. NIR spectroscopy can easily characterise these materials from their X–H bond, however Raman

generally struggles to discriminate between similar carbohydrate species. A specific example of this is the ability of NIR to correctly differentiate between a commonly used diluent, microcrystalline cellulose (MCC), from the disintegrating agent, sodium starch glycolate. However, some excipients may exist as an inorganic material which exhibit weak or more typically no NIR spectrum. An example of this is the commonly used tabletting agent, dibasic calcium phosphate. Here, Raman spectroscopy is the superior technique. Unlike, Raman, NIR spectroscopy also provides a means for water detection. This can be particularly useful to determine the moisture content or hydration state of a material.

This study explores the relative capabilities of Raman and NIR chemical mapping for the analysis of pharmaceutical products. A simplified model system composed of two excipients and one API, which all differed in their elemental composition, was chosen to simulate a real drug product. SEM-EDX analysis was used as an alternative surface imaging technique to confirm the distribution of components and compare with the spectroscopic images.

Experimental

Sample Formulation

The sample tablet was composed of a three-component formulation containing an active ingredient (eletriptan hydrobromide), a common diluent agent (MCC) and a sweetener (saccharin) in a 1:1:1 w/w ratio.

The raw materials were weighed using a METTLER TOLEDO® XP205 analytical balance and the combined mixture was blended using a TURBULA® shaker-mixer (Glen Mills Inc, New Jersey, USA) at a rate of 46 rotations per minute for 5 minutes. A Specac Atlas Auto T8 wafer press (Specac Ltd, Orpington, UK) was used to compact the blend into a wafer. An A2 scoop of the formulation was inserted

into a 10 mm die and compressed to 1 tonne, held for one minute and medium release to 0 tonne. The sample was then polished using a Leica EM Rapid Tablet Mill (Leica, Wetzlar, Germany) to produce an optically flat surface.

Sample Preparation

To ensure the same area was examined by both techniques an approach was used, devised by F. Clarke et al.,[21] to reference coordinate markers between instruments prior to analysis. To prevent movement during analysis, the samples were adhered to a chemical image fusion microscope slide using cyanoacrylate glue. A schematic of the chemical image fusion microscope slide is displayed in Figure 1, along with the coordinate values of the markers obtained from both instruments. This revealed a maximum error of 3 µm (0.03%) in the X direction and 21.1 µm (0.11%) in the Y direction, enabling a reproducibility greater than ±2 pixels in the resultant chemical images. This demonstrated that the error was small, and it was therefore possible to compare the Raman and NIR images with confidence.

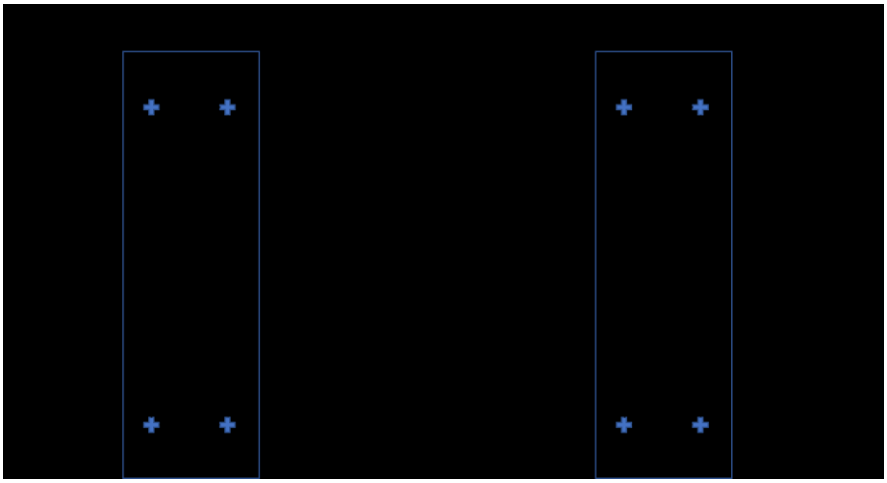

Figure 1. Schematic of the chemical image fusion microscope slide with reference markers. Coordinate values of each crosshair obtained on each instrument are shown in bold along with distances between crosshairs as calculated using the coordinates.

Chemical Mapping Data Collection

All Raman data was collected using a WITec Alpha 500+ CRM (WITec GmbH, Ulm, Germany) Raman microscope. A Perkin Elmer FT-NIR Spectrometer with a FT-(N)IR

microscope (Perkin Elmer, Massachusetts, USA) was used for the NIR mapping experiment. A comparison of the data acquisition parameters is displayed in Table I.

Table I. A comparison of the data acquisition parameters used for the Raman and NIR chemical mapping experiment.

	Raman	**NIR**
Instrument Name	WITec Alpha 500+ CRM	Spotlight400
Excitation Laser / nm	785	-
Spectral Range / cm^{-1}	132.5–1910	3900–7600
Spectral Resolution / cm^{-1}	1	16
Detector	CCD	InGaAs duet detector (16 element array)
Objective	20 x 0.46 NA	15 x 0.60 NA Cassegrainian
Scan area / µm	3000 x 3000	3000 x 3000
Step Size / µm	10	25
Acquisition time / s	0.1	0.05
Number of Scans per Spectrum	1	4
Total Mapping Time	~3.5 hours	~13 min

Chemical Mapping Software and Data Processing

Prior to imaging processing, the Raman datasets were treated with cosmic ray removal and background subtraction to eliminate the effect of cosmic rays and fluorescence in the Raman spectra. Chemical images were prepared using ISys® 5.0 chemical mapping software. Both NIR and Raman datasets were normalised using mean center and scale to unit variance by spectrum to eliminate differences in sample presentation, such as pathlengths. The resultant datasets were then treated with Partial Least Squares-Discriminant Analysis (PLS-DA) II. A reference library of the raw materials was built by obtaining a 1000 µm x 1000 µm Raman and NIR chemical image of compacts of the pure components (eletriptan HBr, MCC and saccharin). Each chemical image contained >1600 spectra which was used to build a PLS classification model for both the Raman and NIR dataset.

The PLS models were applied to the pure component Raman and NIR maps to validate if the model could successfully distinguish between each material. The classification maps, shown in Figure S2, demonstrate the model was able to correctly identify each component in the pure Raman and NIR maps and thus the model was considered suitable for the formulation. Application of the respective PLS model to the chemical images of the sample resulted in a classification score image for each library component. The intensity of each pixel in the classification score image is determined by degree of membership to a particular class (component) by comparing the spectral response at the specific pixel with the reference library spectra. This is given an arbitrary value between 0 and 1, where a score value of 0 represents the absence of a component in a pixel and a score value of 1 demonstrates 100% presence a component. Red, green and blue (RGB) images were obtained by the combining the classification score images for each component. The classification score image of each component chosen for the RGB image was controlled by selecting an area of the classification histogram distribution which represented the distribution and concentration of each material in the formulation. To obtain the most suitable classification score images for each component, various regions of the histogram were explored, and spectral investigation of the white, grey and black pixels were used to determine if the method is representative of the component in the sample.

Quantitative domain size and distribution statistics were obtained by generating binary images of the individual components from the classification images using the mean value pixel distribution. The number of included particles and percentage area covered was determined by the number of particles present and the proportion of the image covered by particles, respectively. The mean equivalent diameter of domains

was calculated by approximating each domain as a perfect circle that occupies the same area as the particle area.

SEM and EDX Data Collection

A Carl Zeiss MA15 (Zeiss, Oberkochen, Germany) scanning electron microscope operated at an accelerating voltage of 20 kV in variable pressure mode was used to examine the sample surface. An electron micrograph was captured at a magnification of X75 using a solid-state back scattered electron detector. The contrast of the image was controlled by the average atomic number of the specimen with bright areas corresponding to materials containing relatively heavier atoms and darker regions containing lighter elements.

The qualitative elemental compositions of the sample surface were determined using an Aztec energy dispersive elemental X-ray microanalysis system (Oxford Instruments, Abington, UK) equipped with an X-Max 80 mm^2 Peltier-cooled X-ray detector. The raw materials of the formulation were also analysed by EDX to obtain reference spectra.

Results and Discussion

A three-component system, composed of two excipients and one API, in a 1:1:1 w/w ratio was used to simulate a real drug product. This was chosen as a compromise between the requirement of the system to be simplistic in nature while still obtaining a spatial distribution of components similar to a real drug product. Eletriptan HBr API ($C_{22}H_{27}BrN_20_2S$), MCC ($C_{14}H_{26}O_{11}$) and saccharin ($C_7H_5NO_3S$) were chosen for the individual components due to each material differing in their chemical nature and elemental composition and thus could be uniquely identifiable by both spectroscopy and SEM/EDX analysis. The structures of each material and their respective Raman and NIR spectra are displayed in Figure 2.

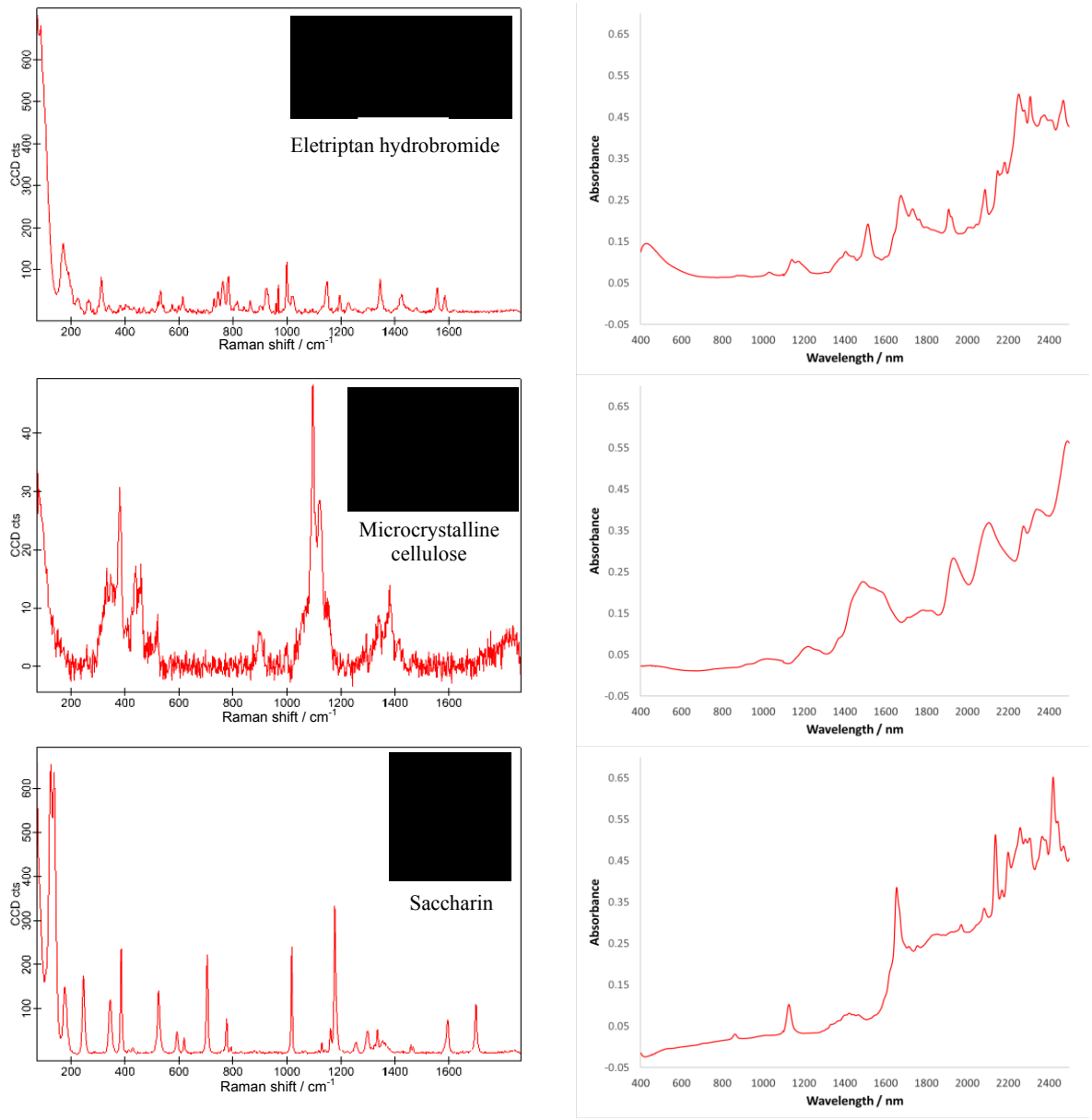

Figure 2. The molecular structure, Raman (left) and near-infrared (right) spectrum of eletriptan HBr (top), microcrystalline cellulose (centre), and saccharin (bottom).

MCC has a characteristically weaker Raman scatter relative to the other components due to its chemical nature and therefore exhibits a relatively poorer signal-to-noise ratio under equivalent data acquisition parameters.

The particle size of the raw components was determined using a QICPIC (Sympatec, Clausthal-Zellerfeld, Germany) dynamic image analysis system equipped with a lens capable of measuring particles in the range of 4.2 – 2888 µm. The volume weighted particle size distribution and the corresponding numerical values are provided in Figure S1 and Table S1, respectively. Eletriptan HBr exhibited the smallest mean particle size by volume at 42.22 µm, while the other two components revealed larger

values greater than 200 μm. The D[v,0.1] value of eletriptan HBr was 21.45 μm, which corresponds to 10% of the particles being smaller than this value. The highest resolution achievable on commercially available NIR mapping systems is 25 μm and therefore it is possible that some pixels acquired by this technique may be mixed resulting in pixel misclassification. Eletriptan HBr has very typical physical properties of an API and therefore was used in the formulation to represent the challenges of acquiring the spatial distribution of APIs in drug products using NIR mapping. A lower lateral spatial resolution of 10 μm was chosen for the Raman instrument as a compromise between a spatial resolution able to visualise the majority of particles, while reducing the data acquisition time required to generate a chemical map.

Raman and Near-Infrared Image Comparison

The chemical images obtained by Raman and NIR chemical mapping are displayed in Figure 3. Initial inspection reveals a very different spatial distribution of components. The domains present in the NIR chemical image appear pixelated and agglomerated together, while the Raman data reveals discrete domains which can be discriminated from one another with a well-defined shape. Closer inspection shows similar domains can be located in both images. For example, the large green domain of saccharin in the bottom left-hand corner and the blue agglomerate of microcrystalline cellulose particles in the left-hand centre of the images.

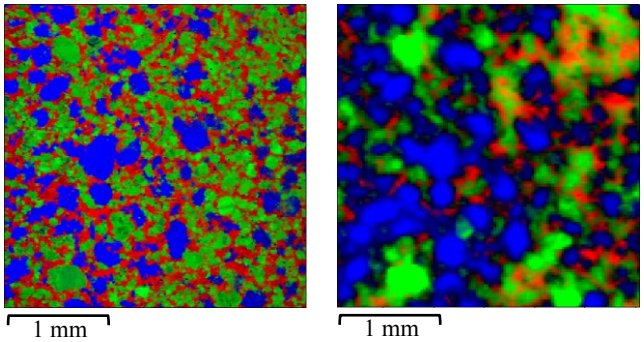

Figure 3. (left) Raman and (right) NIR chemical image where blue = microcrystalline cellulose, green = saccharin and red = eletriptan HBr.

SEM-EDX Validation

An electron micrograph of the tablet surface, displayed in Figure 4, shows a grey-scale image with three different contrasts, corresponding to the three components in the tablet system. Spectral comparison using EDX microanalysis revealed the elemental composition of each region and thus identified the contrast as a particular component (MCC = dark grey, saccharin = medium grey, and eletriptan HBr = light grey). This enables the spatial distribution of components to be easily visualised in the electron micrograph.

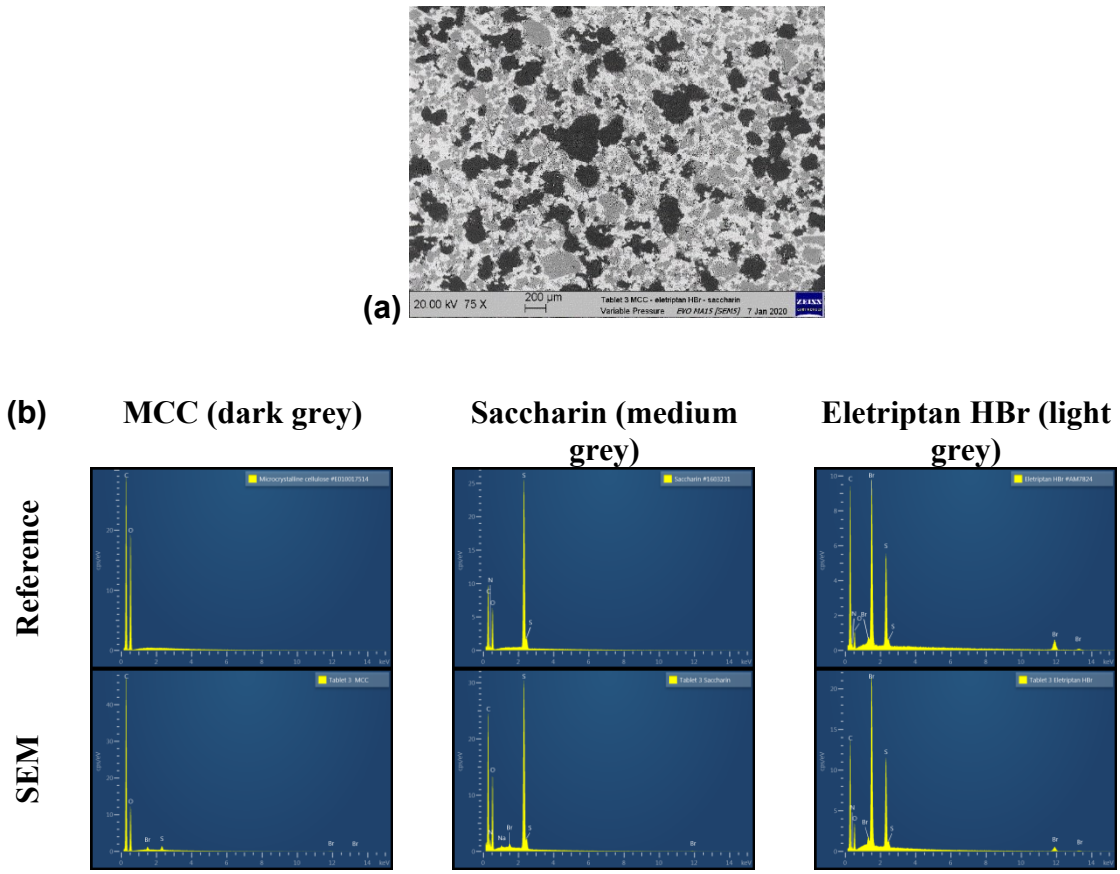

Figure 4. (a) An electron micrograph of the sample surface at a magnification of 75X and (b) a comparison of the EDX spectrum obtained from the raw reference materials and the contrasting domains in the SEM micrograph which identified dark grey =microcrystalline cellulose, medium grey = saccharin and light grey = eletriptan HBr.

An EDX map is a false colour image of the sample surface that can be easily compared to the chemical images obtained spectroscopically. Each material differed in their elemental composition and thus an overlay of the distribution of bromine, sulphur and carbon / oxygen could successfully differentiate between each component. Figure 5 shows the chemical images of the same surface area using Raman and NIR, as well as the EDX map. It was not possible to examine the exact same surface area of sample for SEM-EDX analysis, however distinct domains in the chemical images were located and a larger area was measured. This ensured the whole sample area examined spectroscopically could be compared in the EDX map.

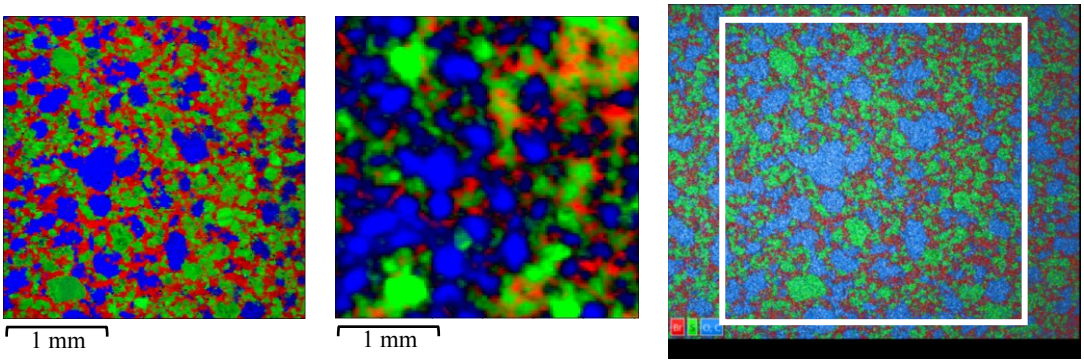

Figure 5. (left) Raman, (centre) NIR and (right) EDX image where blue = microcrystalline cellulose, green = saccharin and red = eletriptan HBr. The white box represents the approximate area measured by the spectroscopic mapping methods.

Inspection of images reveal the Raman and EDX map exhibit a very similar spatial distribution of components. The most notable differences between the images obtained spectroscopically were the size and shape of domains. The Raman image clearly discriminates between domains of each component with a well-defined shape and shows good agreement with the EDX map. The pixelated large domains present in the NIR image suggest this is an inaccurate representation of the distribution of components.

To further compare the differences in the Raman and NIR chemical images, binary images of each component were constructed using the mean value pixel distribution. Binary images of each contrast present in the SEM micrograph were also produced by applying a contrast threshold. The binary images of each component acquired by all three techniques are provided in the supplementary information (Figure S3). As suggested previously, comparison of the binary images reveal the Raman and SEM show the best agreement with regards to domain size, shape and distribution and there is little visual similarity between the NIR and SEM binary images. This further highlights the inability of the NIR chemical image to provide an accurate representation of the spatial distribution of components.

Visual inspection of the binary images reveals there are generally a larger number of domains present in the Raman image, however these domains are typically smaller with a better-defined shape. There are also several small domains present in the Raman image which are absent in the NIR data. These differences are likely to have resulted from the difference in the spatial resolution available by each technique. Under ideal circumstances Raman mapping systems can achieve a lateral spatial resolution of single micrometres, while the volumetric resolution is a much more complicated issue. A step size of 10 μm was chosen for this experiment as a compromise of the data acquisition time and resolution. The maximum XY resolution of many commonly used commercial NIR chemical mapping systems and the spatial resolution used here is 25 μm. The higher resolution available on the Raman instrument enables better discrimination between domains as well as the detection of smaller particles.

The domains present in the NIR image generally appear pixelated and agglomerated together. This is particularly notable for the MCC and saccharin components, which both have a characteristically strong NIR response. The pixelated domains present here are typical of observing spectroscopic response within the core of the sample. Raman instruments are fitted with a confocal aperture which limits the detection of spectral response from out-of-focus light, and thus data is collected from a smaller volume at the microscope focal point. NIR instruments do not have this ability, and data is collected from a larger volume.[22] The NIR binary image of eletriptan HBr, displayed in Figure S3, appears to underestimate the concentration of this component, particularly on the left-hand side of the image. Eletriptan HBr is an acid salt of an organic molecule which has a relatively weaker NIR spectrum compared with the other components. Interestingly, the NIR distribution of MCC and saccharin

appear oversized and pixelated in this region relative to what is observed in the Raman image. It is likely that the poor NIR response from eletriptan HBr on the sample surface is being overpowered by the strong response of MCC and saccharin within the sample core. This is amplified by larger sample volume detected by NIR due to the lack of confocality in the system.

Quantitative Image Comparison

To evaluate quantitative differences between chemical images, the number and size of the domains of each component in the chemical images were determined from the binary images and displayed in Table II. The equivalent diameter of a domain is estimated by assuming each domain is a perfect circle that occupies the same area as the domain area.

To quantify the differences in the SEM-EDX data, the full image was cropped to represent the sample area measured in the NIR and Raman mapping experiment. As discussed earlier, it was not possible to measure the exact same area using this technique and therefore the values quantified will not be completely comparable to the spectroscopically obtained maps. Instead, the purpose of this was to provide some indication of the size and distribution of each component within the formulation to gain a further understanding as to which spectroscopic image best represents the sample surface. The cropped SEM-EDX images used for quantitative analysis is provided in Figure S4.

Table II. A table displaying the number and size of the domains of each component in Raman,NIR and SEM-EDX chemical images.

	Data Acquisition Method	Number of Included Particles	Percentage Area Covered / %	Mean Area / μm^2	Mean Equivalent Diameter / μm
MCC	**Raman**	360	26.73	668.1	53.01
	NIR	44	27.95	2887	185.28
	SEM-EDX	508	31.68	401.76	44.83
Eletriptan HBr	**Raman**	416	36.70	793.9	50.75
	NIR	103	17.67	617.5	94.91
	SEM-EDX	365	32.75	580.63	56.90
Saccharin	**Raman**	460	36.78	719.7	56.68
	NIR	59	27.16	1657	152.48
	SEM-EDX	357	45.99	833.68	43.09

As expected from the binary images, the Raman image generally exhibits a larger number of domains for all components and is more comparable to the SEM-EDX data.. The magnitude in difference is notable and suggests, for this particular formulation, that the higher resolution of the Raman instrument is advantageous. This provides the ability to discriminate between individual components and gain an enhanced understanding of the spatial distribution of components and individual domain size and shape.

The differences in domain size across images have also been quantified by comparing the estimated mean equivalent diameter of domains. Most interestingly, the average size of MCC domains in the NIR image are over three-fold larger compared with the Raman and SEM-EDX data. This was also observed in the binary images of MCC and is the largest difference seen across all three-components. This suggests that this difference is due to the chemical nature of the material. MCC is an unsaturated organic material consisting of a number of heteronuclear bonds which have the ability to induce a dipole moment during molecular vibrations. MCC therefore has a characteristically strong NIR response. The absence of aromatic and / or olefin functionality in the chemical structure classifies MCC as a weak Raman scatterer. As

suggested earlier, it is likely that the overestimation and large pixelated domains of MCC in the NIR images are due to the detection of the strong NIR response of MCC within the core of the sample. This is the major limitation of NIR chemical mapping, such that if the sampling probe volume is greater than the domain volume, the spectral response at a single pixel may contain a mixture of components. It is the material that has the strongest spectral response which is chosen to represent the pixel. Due to the differing properties of components within a formulation, this may not be the material at the sample surface and instead chemical maps may represent an inaccurate distribution of components. This is not the case in the Raman image due to the combination of MCC exhibiting a relatively weaker response and confocality in the measurement reducing the data collection volume. However, despite the characteristically weak spectrum, the MCC percentage area covered in the two images is comparable suggesting Raman is sufficient at detecting this organic compound.

The same trend is generally seen for saccharin however the magnitude is far smaller due to saccharin characteristically having a fairly strong NIR and Raman response. This is due to the molecular structure containing both heteronuclear bonds (such as -NH) and aromatic functionality. Here, the discrepancy in the average domain size is likely due to a combination of the lower spatial resolution and deeper penetration depth of the NIR radiation.

The percentage area covered for eletriptan HBr measured by NIR is underestimated by 2-fold relative to the Raman and SEM-EDX data. This highlights the challenge regarding the large sample volume collected in NIR experiments and its consequential effect on detecting relatively weak NIR absorbers.

Overall, the Raman domain size statistics is most comparable to the SEM-EDX data. There are some differences in values, however this is expected due to the slight

differences in the sample area examined and the higher lateral spatial resolution available with SEM-EDX analysis. However, the magnitude of each value appears to be similar across the Raman and SEM-EDX data, while the NIR statistics are inconsistent with these values. This further suggests the superiority of Raman mapping to obtain information regarding the size and shape of individual domains.

To further quantitively assess the spatial distribution of components, the number of domains and percentage statistics for each quadrant of the chemical image is presented in the supplementary material (Table S2). Generally, the Raman image contains a greater percentage coverage for each component. The most significant difference between images for MCC is seen in the third quadrant, where the Raman image has an almost two-fold coverage compared with the NIR image. This is consistent with the additional small domains present in the Raman data. A similar trend is also seen for saccharin where the largest difference is seen in quadrant 1 and 2. More significantly, the largest difference in percentage cover statistics for eletriptan HBr is seen in the first and second quadrant. This difference was noted earlier in the binary images where this region of the NIR chemical image is populated with large pixelated domains of MCC. This further suggests that the intense NIR response of MCC in the sample core may be dominating the relatively weaker response of the inorganic API at the surface. The absence of confocality appears to play a major role in this discrepancy.

Raman Spatial Resolution Comparison

To determine the effect of the depth of penetration in resultant NIR maps, a Raman map was also acquired at lateral spatial resolution of 25 μm. Figure 7 shows a comparison of a Raman map of the same sample collected at (a) 10 μm and (b) 25 μm (lateral spatial resolution) with (c) an NIR image of the same area (25 μm step

size). Visual inspection of the images demonstrates a clear difference in the distribution of components between the Raman and NIR maps. Both Raman images shows a similar spatial distribution of components with similar domain shapes and sizes. The domains present in the lower spatial resolution Raman map appear less discriminated and slightly pixelated at edges of the domain. The absence of large pixelated domains agglomerated together in the Raman image suggests this artefact in the NIR image is mainly due to the large penetration depth of the NIR radiation, resulting in overestimation of components which are strongly NIR absorbing.

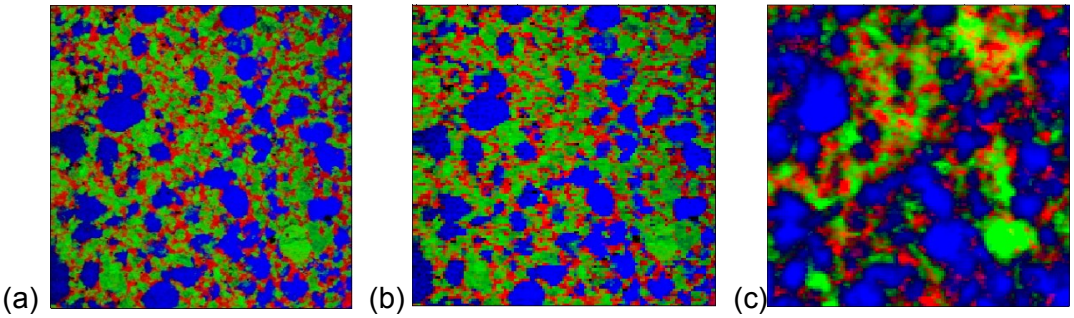

Figure 6. Raman image acquired with a lateral spatial resolution of (a) 10 microns and (b) 25 microns and (c) a NIR image acquired with a lateral spatial resolution of 25 microns, where blue = microcrystalline cellulose, green = saccharin and red = eletriptan HBr.

To quantitatively examine the difference in the Raman and NIR images, the number and size of domains were calculated and presented in Table III. The most notable difference is seen in the strongly NIR absorbing MCC component, where the NIR image suggests larger and fewer domains compared with what is present in both Raman images. There is a difference in the number and size of MCC domains between the Raman images collected at a step size of 10 μm and 25 μm, however the magnitude of the discrepancy is smaller suggesting the large difference seen in the NIR data is a combination of both a lower spatial resolution but also an increased sample volume provided by the NIR system. This is supported by a smaller difference seen for saccharin, which is a relatively weaker NIR absorber compared to MCC and more interestingly, little difference in the domain size for eletriptan HBr which is known

to be a weak NIR absorber. This highlights the challenges associated with NIR chemical imaging for a sample which contains a mixture of strong to weak NIR absorbers. The large penetration depth of the NIR radiation leads to overestimation of strongly absorbing NIR components through the detection of material beneath the sample surface inhibiting the ability to obtain a chemical image at the surface of a sample.

Table III. A table displaying the number and size of the domains of each component in Raman chemical images acquired with a 10 μm and 25 μm lateral spatial resolution.

		Lateral Spatial Resolution / μm	Number of Included Particles	Percentage Area Covered / %	Mean Area / μm^2	Mean Equivalent Diameter / μm
MCC	**Raman**	10	272	30.31	1003.02	66.29
		25	118	31.16	950.63	128.15
	NIR	25	38	34.10	3230.92	223.46
Saccharin	**Raman**	10	424	35.86	761.23	52.81
		25	155	36.46	846.78	94.80
	NIR	25	85	22.26	942.94	97.27
Eletriptan HBr	**Raman**	10	591	30.69	467.31	47.37
		25	277	28.50	370.40	81.44
	NIR	25	118	22.31	680.51	96.72

Sample Representation

To ensure the chemical images acquired are representative of each spectroscopic technique, additional chemical images of the sample cross-sectioned at various depths were examined. This is an essential step for using chemical mapping as a tool to estimate the component composition within a tablet due to current techniques only involving the examination of a single two-dimensional slice. Mixing is a crucial step in the manufacturing of pharmaceutical tablets to ensure components are homogenously distributed within a drug product. It is very difficult to achieve a perfectly mixed formulation in practice and thus several samples at various depths are required to obtain an accurate estimate of the component composition.

Chemical images of the tablet acquired at 30 μm depth intervals into the sample were obtained by physically polishing the surface using a Leica EM Rapid Tablet Mill (Leica, Wetzlar, Germany) to ensure the cross-section examined in this paper is representative of the overall tablet composition. The chemical images, displayed in Figure 7, reveal a similar spatial distribution of components to the chemical images examined in this paper.

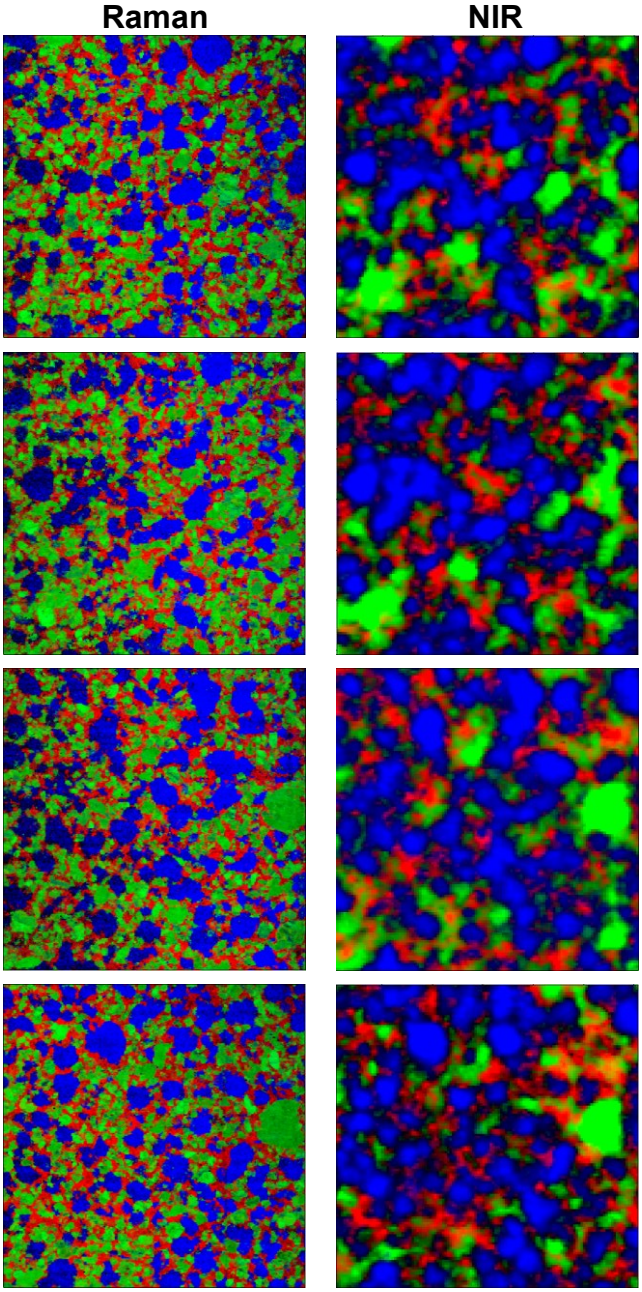

Figure 7. Chemical images of the three-component system acquired at 30 μm (top), 60 μm (upper centre), 90 μm (lower centre), and 120 μm (bottom) deep into the sample by (left) Raman and (right) NIR chemical mapping. Examination of the same sample area was achievable by both techniques using chemical image fusion microscope slides.

Generally, the Raman image consists of well-resolved and discriminated domains of each component whereas the domains present in the NIR image appear pixelated and agglomerates together. Again, the NIR images appear to be heavily dominated by large domains of MCC and saccharin and the distribution of eletriptan HBr appears to be underestimated.

Conclusion

This study successfully demonstrated the difference in the capabilities of Raman and NIR chemical mapping for pharmaceutical analysis. Qualitative and quantitative inspection of the chemical images revealed very different spatial distributions of components with regards to domain size and shape. The Raman image exhibited sharper and better discriminated domains of the individual components whereas the NIR image was heavily dominated by large pixelated domains of MCC and saccharin.

Evaluation of the sample surface by SEM-EDX analysis revealed a spatial distribution of components comparable to the Raman image with similar domain size and shape. This demonstrated the superiority of Raman to obtain a chemical image representative of the sample surface with the capabilities to provide a better approximation of domain size and shape. However, the long acquisition times required for Raman mapping experiments mean this technique may not be suitable for all samples, particularly dynamic specimens or investigations which require many samples to be analysed. The rapid data acquisition time achievable by NIR mapping may be valuable as a less precise method to analyse many samples where regions of interest can be identified and more extensively examined using Raman. Despite the vast differences in the quality of the chemical images, NIR chemical mapping is still widely used in the pharmaceutical industry as a useful tool to rapidly characterise differences in the spatial distribution of components in troubleshooting investigations.

Ultimately, the choice of vibrational spectroscopic mapping or imaging technique for a particular formulation will depend on the time available for analysis, the spatial resolution required, the desired information to be obtained and the chemical nature of the components.

Acknowledgements

This work was supported by Global Technology and Engineering, Pfizer Global Supply.

Declaration of Conflicting Interests

The author declares that they have no conflicts of interest.

References

1. S. Stewart, R.J. Priore, M.P. Nelson, J.P. Treado. “Raman Imaging”. Annu. Rev. Anal. Chem. 2012. 5(1): 337-360.
2. S. Šašić. “An in-depth analysis of Raman and near-infrared chemical images of common pharmaceutical tablets”. Appl. Spectrosc. 2007. 61(3): 239-250.
3. F. Liu, R. Lizio, U.J. Schneider, H.-U. Petereit, P. Blakey, A.W. Basit. “SEM/EDX and confocal microscopy analysis of novel and conventional enteric-coated systems”. Int. J. Pharm. 2009. 369(1): 72-78.
4. J.I. Goldstein, D.E. Newbury, P. Echlin, D.C. Joy, C.E. Lyman, E. Lifshin, L. Sawyer, J.R Michael. “Image Formation and Interpretation”. In: Scanning Electron Microscopy and X-ray Microanalysis. Boston, MA, USA: Springer, 1992. Vol. 3, Chap. 4, 149-271.
5. G. Nichols. “Anomalous atomic number contrast in compositional backscattered electron images of organic compounds due to cathodoluminescence”. The Microscope. 2011. 59(4): 147-163.

6. N. Scoutaris, K. Vithani, I. Slipper, B. Chowdhry, D. Douroumis. “SEM/EDX and confocal Raman microscopy as complementary tools for the characterization of pharmaceutical tablets”. Int. J. Pharm. 2014. 470(1): 88-98.
7. U. Schmidt, P. Ayasse, O. Hollricher. “RISE Microscopy: Corrective Raman and SEM Imaging”. Microsc. Today. 2014. 22(6): 36-39.
8. L.R. Hilden, C.J. Pommier, S.I.F. Badawy, E.M. Friedman. “NIR chemical imaging to guide/support BMS-561389 tablet formulation development”. Int. J. Pharm. 2008. 353(1): 283-290.
9. C. Gendrin, Y. Roggo, C. Collet. “Content uniformity of pharmaceutical solid dosage forms by near infrared hyperspectral imaging: A feasibility study”. Talanta. 2008. 73(4): 733-741.
10. Y. Roggo, N. Jent, A. Edmond, P. Chalus, M. Ulmschneider. “Characterizing process effects on pharmaceutical solid forms using near-infrared spectroscopy and infrared imaging”. Eur. J. Pharm. Biopharm. 2005. 61(1): 100-110.
11. S.V. Hammond, F.C. Clarke. “Near-infrared microspectroscopy”. In: J.M Chalmers, P.R. Griffins, editors. Handbook of Vibrational Spectroscopy. London, UK: John Wiley & Sons, 2002. Vol. 2, 1405-1418.
12. C. Gendrin, Y. Roggo, C. Spiegel, C. Collet. “Monitoring galenical process development by near infrared chemical imaging: One case study”. Eur. J. Pharm. Biopharm. 2008. 68(3): 828-837.
13. S. Šašić, A. Kong, G. Kaul. “Determining API domain sizes in pharmaceutical tablets and blends upon varying milling conditions by near-infrared chemical imaging”. Anal. Methods. 2013. 5(9): 2360-2368.

14. S. Šašić, W. Yu, L. Zhang. “Monitoring of API particle size during solid dosage form manufacturing process by chemical imaging and particle sizing”. Anal. Methods. 2011. 3(3): 568-574.
15. J. Dubois, E.N. Lewis. “Advanced Troubleshooting of Dissolution Failure”. 2009. 38-45. Available from: www.pharmaceuticalonline.com
16. C.R. Lyon, D.S. Lester, E.N. Lewis, E. LEE, L.X. Yu, E.H. Jefferson, A.S. Hussain. “Near-infrared spectral imaging for quality assurance of pharmaceutical products: analysis of tablets to assess powder blend homogeneity”. AAPS PharmSciTech. 2002. 3(3): 422-434
17. C. Gendrin, Y. Roggo, C. Collet. “Pharmaceutical applications of vibrational chemical imaging and chemometrics: A review”. J. Pharm. Biomed. Anal. 2008. 48(3): 533-553.
18. K. Hashimoto, V.R. Badarla, A. Kawai, T, Ideguchi. “Complementary vibrational spectroscopy”. Nat. Commun. 2019. 10(1): 4411.
19. R. Salzer, H.W. Siesler. “Infrared and Raman Instrumentation for mapping and imaging”. In: Infrared and Raman spectroscopic imaging, London, UK: John Wiley & Sons, 2014. Vol. 1, Chap. 1, 5-37.
20. K.C. Gordon, C.M. McGoverin. “Raman mapping of pharmaceuticals”. Int. J. Pharm. 2011. 417(1): 151-162.
21. F.C. Clarke, M.J. Jamieson, D.A Clark, S.V. Hammond, R.D. Jee, A.C. Mofatt. “Chemical Image Fusion. The Synergy of FT-NIR and Raman Mapping Microscopy To Enable a More Complete Visualization of Pharmaceutical Formulations”. Anal. Chem. 2001. 73(10): 2213-2220.
22. F.C. Clarke, S.V. Hammond, R.D. Jee, A.C. Moffat. “Determination of the Information Depth and Sample Size for the Analysis of Pharmaceutical Materials

Using Reflectance Near-Infrared Microscopy". Appl. Spectrosc. 2002. 56(11): 1475-1483.

Extra Supplementary Information

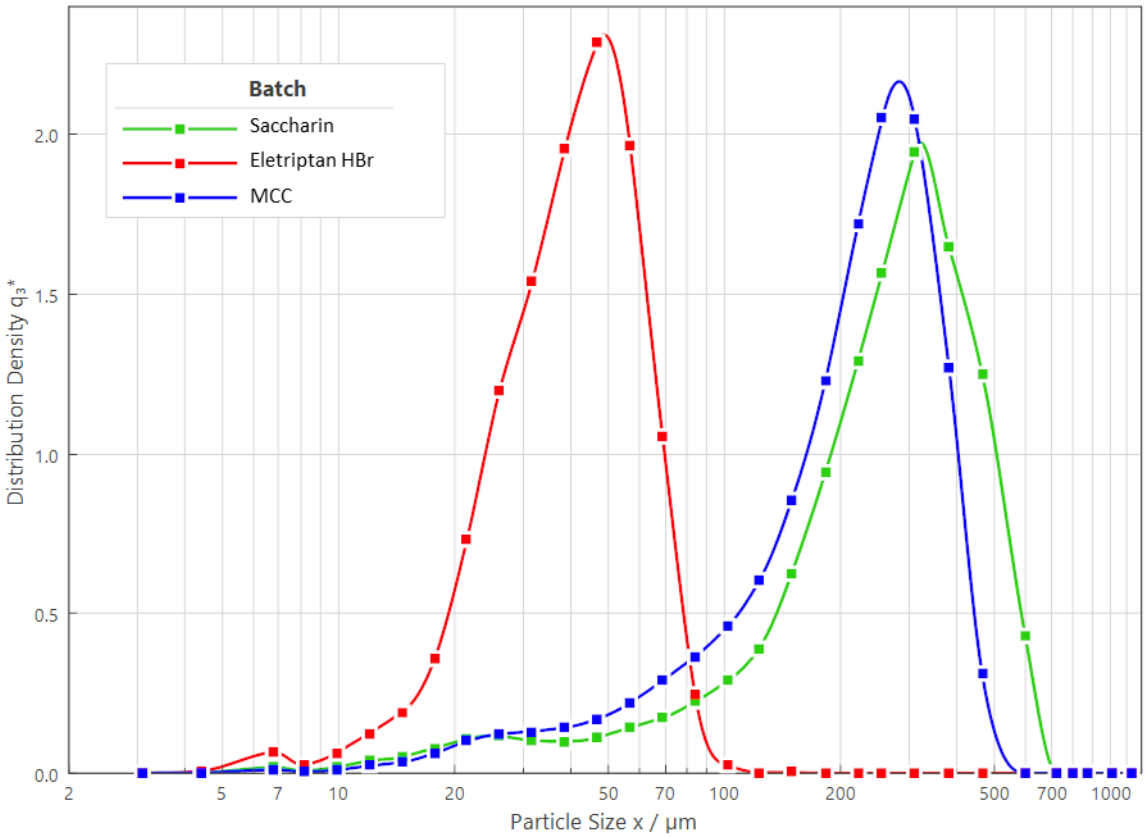

Figure S1. QICPIC volume particle size distributions histogram of the raw materials where red = eletriptan hydrobromide, blue = microcrystalline cellulose and green = saccharin.

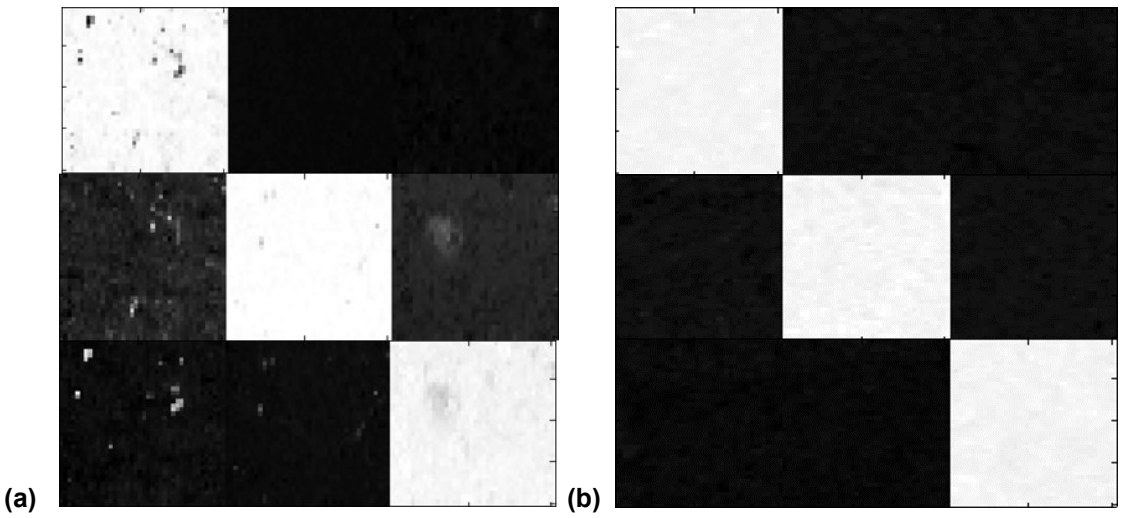

Figure S2. PLS Classification maps of the pure components, (left) microcrystalline cellulose, (centre) Eletriptan hydrobromide and (right) saccharin, at (top) class one – microcrystalline cellulose, (middle) class two - saccharin and (bottom) class three – eletriptan hydrobromide, for the (a) Raman and (b) NIR PLS model, where white pixels represent the belonging to the class.

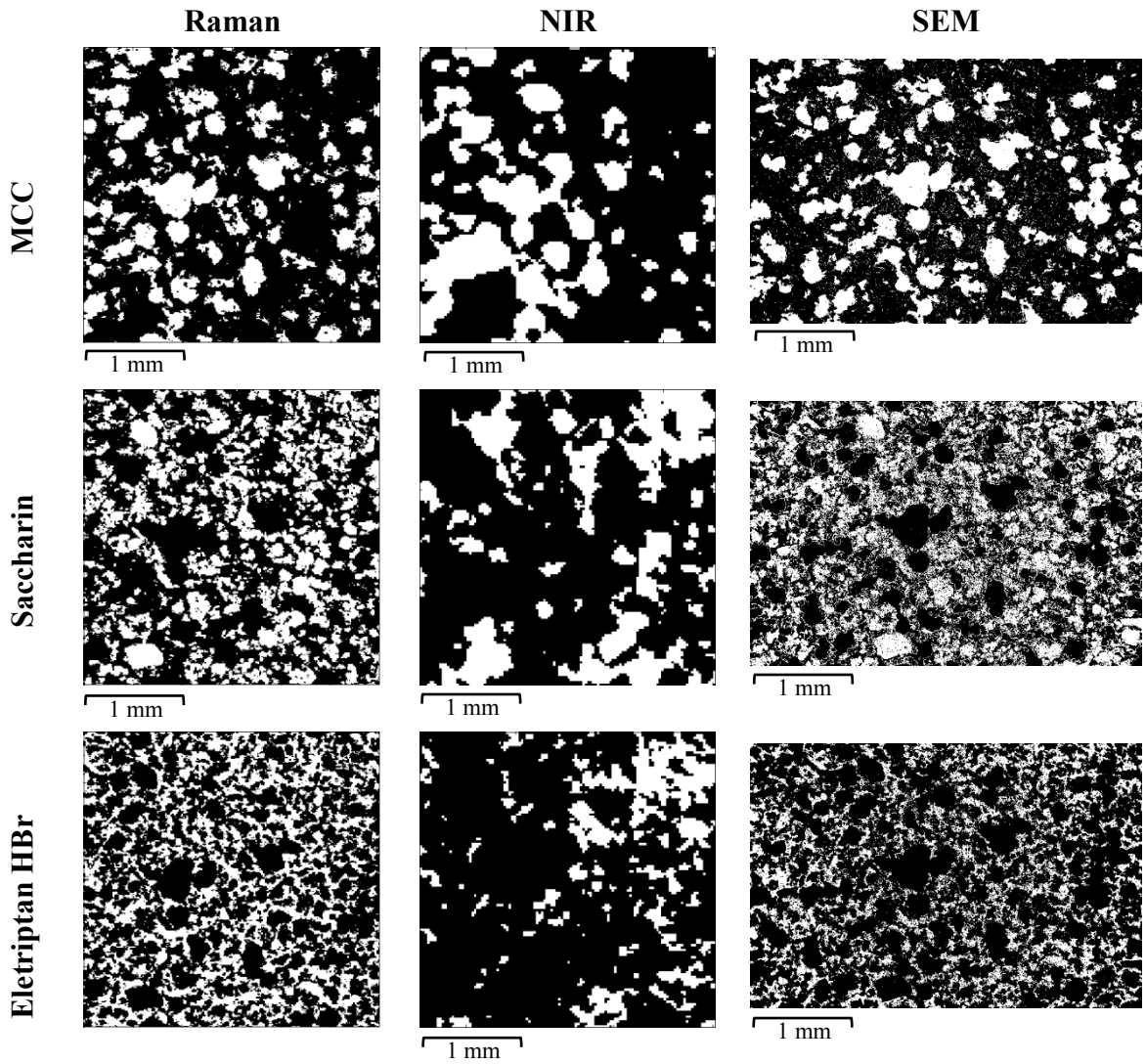

Figure S3. Binary image of the spatial distribution of the individual components obtained by Raman,NIR and SEM-EDX.

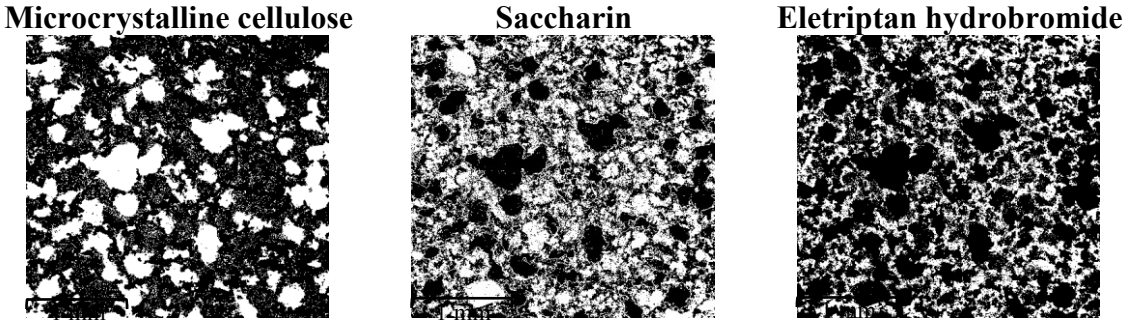

Figure S4. Cropped binary SEM-EDX images used for quantitative analysis.

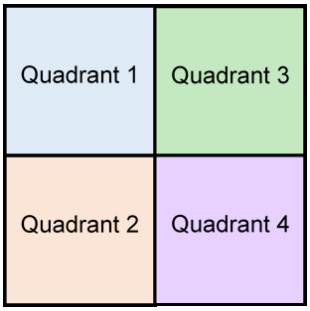

Figure S5. A schematic identifying each quadrant number in the chemical image.

Table S1. QICPIC volume particle size values of the raw materials.

Material	D[v,0.1] / µm	D[v,0.5] / µm	D[v,0.9] / µm	Mean by Volume / µm
Eletriptan hydrobromide	21.45	41.11	64.42	42.22
Saccharin	277.71	486.09	486.09	281.85
Microcrystalline Cellulose	69.61	227.75	359.90	225.20

Table S2. A table showing the domain distribution statistics for each component in the Raman, NIR and SEM-EDX chemical images, where Q = quadrant.

		Number Statistics				Percentage Cover Statistics			
	Data Acquisition Method	Q1	Q2	Q3	Q4	Q1	Q2	Q3	Q4
MCC	Raman	92	86	86	106	31.99	33.08	20.31	21.54
	NIR	16	4	14	17	34.01	48.87	11.78	17.06
	SEM-EDX	128	121	131	135	36.18	35.46	27.30	28.08
Eletriptan HBr	Raman	140	103	95	110	24.87	36.67	38.95	36.29
	NIR	23	34	24	34	6.87	6.41	40.42	18.42
	SEM-EDX	113	104	78	94	29.27	30.43	36.20	34.98
Saccharin	Raman	115	121	119	133	36.08	31.71	40.17	39.07
	NIR	20	16	13	16	19.79	18.96	38.81	32.40
	SEM-EDX	87	110	104	87	45.68	43.99	47.16	47.18